

Bottomonia in the Quark Gluon Plasma

Michael Strickland

Physics Department, Gettysburg College, Gettysburg, PA 17325 United States

Abstract. I review recent calculations of the suppression of bottomonium states in heavy ion collisions. A non-relativistic potential is used which is complex valued. This allows one to extract the binding energies and decay widths of the ground and excited states of bottomonium as a function of the typical plasma particle momentum and momentum-space anisotropy. The decay widths determined are used as input and integrated over space-time taking into account the dynamical evolution of the typical particle momentum and momentum-space anisotropy. The suppression of $\Upsilon(1s)$, $\Upsilon(2s)$, $\Upsilon(3s)$, χ_{b1} , and χ_{b2} is obtained as a function of centrality, rapidity, and transverse momentum. The obtained results are compared with data from the STAR and CMS collaborations.

1. Introduction

In November of 2010 the Large Hadron Collider (LHC) at the European Organization for Nuclear Research (CERN) achieved its first relativistic heavy ion collisions of lead nuclei (Pb-Pb). The goal of such experiments is to recreate conditions which only existed in the early universe before the formation of hadrons. The LHC is searching for evidence of the creation of a primordial state of matter called the quark gluon plasma (QGP) which comprised the entire universe until approximately 10^{-5} seconds after the big bang when the temperature of the universe was on the order of 10^{12} Kelvin. The LHC experiment is attempting to recreate such temperatures by colliding lead nuclei at $\sqrt{s_{NN}} = 2.76$ TeV/nucleon whereas the lower energy Relativistic Heavy Ion Collider (RHIC) at Brookhaven National Laboratory has been colliding gold nuclei at $\sqrt{s_{NN}} = 200$ GeV/nucleon. In addition to simply crossing the threshold for the creation of a quark gluon plasma, the experiments are also making detailed measurements of the collision products in order to determine fundamental properties of the QGP. The resulting data are being compared to theoretical calculations based on quantum chromodynamics (QCD) which describes the interactions of quarks and gluons.

At high temperatures one expects the emergence of Debye screening of the interaction between quarks and gluons. This leads to the dissolution of hadronic bound states [1]. A particularly interesting subset of hadronic states consists of those comprised of heavy quarks, since the spectrum of low lying states can be found using potential-based non-relativistic treatments. Based on such potential models there were early predictions [2, 3] that J/ψ production would be suppressed in heavy ion collisions relative to the corresponding production in proton-proton collisions scaled by the number of nucleons participating in the collision. In recent years there have been important theoretical advances in the understanding of heavy quark states at finite temperature using analytic techniques [4–12] and lattice QCD [13–21]. Most recently, interest has shifted to bound states of bottom and anti-bottom quarks (bottomonium) for the following reasons

- (i) Bottom quarks ($m_b \simeq 4.2$ GeV) are more massive than charm quarks ($m_c \simeq 1.3$ GeV) and as a result the heavy quark effective theories underpinning phenomenological applications are on much surer footing.
- (ii) Due to their higher mass, the effects of initial state nuclear suppression are expected to be smaller than for the charmonium states [22].
- (iii) The masses of bottomonium states ($m_\Upsilon \approx 10$ GeV) are much higher than the temperatures ($T \lesssim 1$ GeV) generated in relativistic heavy ion collisions. As a result, bottomonium production will be dominated by initial hard scatterings.
- (iv) Since bottom quarks and anti-quarks are relatively rare within the plasma, the probability for regeneration of bottomonium states through recombination is much smaller than for charm quarks.

As a result one expects the bottomonium system to be a cleaner probe of the quark gluon plasma than the charmonium system for which the modeling has necessarily become quite involved. For this reason we will focus on the bottomonium states and only consider the thermal suppression of these states, ignoring initial state effects and any possible thermal generation or recombination. In this conference proceedings we will review recent theoretical calculations of bottomonium suppression at energies probed in relativistic heavy ion collisions at RHIC and LHC. We will present an overview of the important aspects of the calculation and refer the reader to Refs. [23, 24] for details. We will compare our predictions for inclusive $\Upsilon(1s)$ and $\Upsilon(2s)$ suppression with recent data to from the CMS and STAR collaborations.

2. Theoretical methods

In the last few years there have been important theoretical developments in the theoretical treatment of heavy quarkonium in the quark gluon plasma. First among these are the first-principles calculations of imaginary-valued contributions to the heavy quark potential. The first calculation of the leading-order perturbative imaginary part of the potential due to gluonic Landau damping was performed by Laine et al. [5]. Subsequently, an additional imaginary-valued contribution to the potential coming from singlet to octet transitions has also been computed using the effective field theory approach [9]. These imaginary-valued contributions to the potential are related to quarkonium decay processes in the plasma. The consequences of such imaginary parts on heavy quarkonium spectral functions [25, 26], perturbative thermal widths [5, 27], quarkonia at finite velocity [28], in a T-matrix approach [4, 8, 29–31], and in stochastic real-time dynamics [32] have recently been studied.

Additionally, there have been significant advances in the dynamical models used to simulate plasma evolution. In particular, there has been a concerted effort to understand the effects of plasma momentum-space anisotropies generated by the rapid longitudinal expansion of the matter along the beamline direction. The resulting dynamical models are now able to describe the anisotropic hydrodynamical evolution using full (3+1)-dimensional simulations [33–38]. This is important because momentum-space anisotropies can have a significant impact on quarkonium suppression since in regions of high momentum-space anisotropy one expects reduced quarkonium binding [7, 10–12, 39]. In Refs. [23, 24] the dynamical evolution of the anisotropic plasma was combined with the real and imaginary parts of the binding energy obtained using modern complex-valued potentials.

2.1. Anisotropic potential model and binding energies

Early on it was shown that ideal relativistic hydrodynamics is able to reproduce the soft collective flow of the matter and single particle spectra produced at RHIC [40–43]. Based on this, there was a concerted effort to develop a systematic framework for describing the soft collective motion.

This effort resulted in a number of works dedicated to the development and application of relativistic viscous hydrodynamics to relativistic heavy ion collisions [44–62].

One of the weakness of the traditional viscous hydrodynamics approach is that it relies on an implicit assumption that the system is close to thermal equilibrium which implies that the system is also very close to being isotropic in momentum space. However, one finds during the application of these methods that this assumption breaks down at the earliest times after the initial impact of the two nuclei due to large momentum-space anisotropies in the p_T - p_L plane which can persist for many fm/c [63]. In addition, one finds that near the transverse and longitudinal edges of the system these momentum-space anisotropies are large at all times [35, 36, 63]. Similar conclusions have been obtained in the context of strongly coupled systems where it has been shown using the conjectured AdS/CFT correspondence one achieves viscous hydrodynamical behavior at times when the system still possesses large momentum-space anisotropies and that these anisotropies remain large throughout the evolution [64–70]. Based on these results one is motivated to apply a dynamical framework that can accommodate potentially large momentum-space anisotropies.

In order to take into account plasma momentum-space anisotropy, the phase-space distribution of gluons in the local rest frame is assumed to be given by [7, 71–74]

$$f(t, \mathbf{x}, \mathbf{p}) = f_{\text{iso}} \left(\sqrt{\mathbf{p}^2 + \xi(\mathbf{p} \cdot \mathbf{n})^2 / p_{\text{hard}}} \right), \quad (1)$$

where f_{iso} is an isotropic distribution which in thermal equilibrium is given by a Bose-Einstein distribution, ξ is the momentum-space anisotropy parameter, and p_{hard} is a momentum scale which specifies the typical momentum of the particles in the plasma and can be identified with the temperature in the limit of thermal isotropic ($\xi=0$) equilibrium. The two parameters p_{hard} and ξ can, in general, depend on proper time and position; however, we do not indicate this explicitly for compactness of notation.

In general one finds that the heavy quark potential has real and imaginary parts, $V = \Re[V] + i\Im[V]$. One can determine the real part of the heavy-quark potential in the non-relativistic limit from the Fourier transform of the 00-component of the static gluon propagator. In an anisotropic plasma with a distribution function given by Eq. (1) one finds [10], at leading order in the strong coupling constant,

$$V(\mathbf{r}, \xi) = -g^2 C_F \int \frac{d^3 \mathbf{p}}{(2\pi)^3} e^{i\mathbf{p} \cdot \mathbf{r}} \Delta^{00}(\omega = 0, \mathbf{p}, \xi), \quad (2)$$

$$= -g^2 C_F \int \frac{d^3 \mathbf{p}}{(2\pi)^3} e^{i\mathbf{p} \cdot \mathbf{r}} \frac{\mathbf{p}^2 + m_\alpha^2 + m_\gamma^2}{(\mathbf{p}^2 + m_\alpha^2 + m_\gamma^2)(\mathbf{p}^2 + m_\beta^2) - m_\delta^4}, \quad (3)$$

where g is the strong coupling constant and $C_F = (N_c^2 - 1)/(2N_c)$ is the quadratic Casimir of the fundamental representation of $SU(N_c)$. The mass scales m_α , m_β , m_γ , and m_δ are listed in Ref. [10]. One can factorize the denominator of (3) by introducing

$$2m_\pm^2 \equiv M^2 \pm \sqrt{M^4 - 4(m_\beta^2(m_\alpha^2 + m_\gamma^2) - m_\delta^4)}, \quad (4)$$

with $M^2 \equiv m_\alpha^2 + m_\beta^2 + m_\gamma^2$ [71]. This allows us to write

$$V(\mathbf{r}, \xi) = -g^2 C_F \int \frac{d^3 \mathbf{p}}{(2\pi)^3} e^{i\mathbf{p} \cdot \mathbf{r}} \frac{\mathbf{p}^2 + m_\alpha^2 + m_\gamma^2}{(\mathbf{p}^2 + m_+^2)(\mathbf{p}^2 + m_-^2)}. \quad (5)$$

In general one must evaluate (5) numerically. The integration can be reduced to a two-dimensional integral over a polar angle, θ , and the length of the three-momentum, p . However,

there can be poles in the integration domain due to the fact that m_-^2 can be negative for certain polar angles and momenta [71]. These poles are first order and can be dealt with using a principle-part prescription. After evaluating the integral numerically, one finds that the resulting potential is very well described by a Debye-screened Coulomb potential with an anisotropic Debye mass μ

$$\Re[V(r)] = -\frac{g^2 C_F}{4\pi r} e^{-\mu r}, \quad (6)$$

where

$$\left(\frac{\mu}{m_D}\right)^{-4} = 1 + \xi \left(a - \frac{2^b(a-1) + (1+\xi)^{1/8}}{(3+\xi)^b} \right) \left(1 + \frac{c(\theta)(1+\xi)^d}{(1+e\xi^2)} \right), \quad (7)$$

The coefficients a-e are fixed by (a) requiring that the small and large anisotropy limits of the analytic potential are reproduced and (b) fitting to the numerical results obtained by direct integration of Eq. (5) [24].

Here we will focus on a model in which the real part of the potential is obtained from internal energy of the system since models based on the free energy seem to be incapable of reproducing either the LHC or RHIC $R_{AA}[\Upsilon]$. The real part of the potential is given by [24]

$$\Re[V] = -\frac{a}{r} (1 + \mu r) e^{-\mu r} + \frac{2\sigma}{\mu} [1 - e^{-\mu r}] - \sigma r e^{-\mu r} - \frac{0.8\sigma}{m_Q^2 r}, \quad (8)$$

where $a = 0.385$ and $\sigma = 0.223 \text{ GeV}^2$ [75] and the last term is a temperature- and spin-independent finite quark mass correction taken from Ref. [76]. In this expression $\mu = \mathcal{G}(\xi, \theta)m_D$ is an anisotropic Debye mass where \mathcal{G} is a rather complicated function (see Eq. (7) above) which depends on the degree of plasma momentum-space anisotropy, ξ , and the angle of the line connecting the quark-antiquark pair with respect to the beamline direction, θ , and m_D is the isotropic Debye mass [24]. In the limit $\xi \rightarrow 0$ one has $\mathcal{G} = 1$. In the figures in the results section, results obtained with Eq. (8) are often labeled as “Potential Model B”.

The imaginary part of the potential $\Im[V]$ is obtained from a leading order perturbative calculation which was performed in the small anisotropy limit

$$\Im[V] = -\alpha_s C_F T \{ \phi(r/m_D) - \xi [\psi_1(r/m_D, \theta) + \psi_2(r/m_D, \theta)] \}, \quad (9)$$

where ϕ , ψ_1 , and ψ_2 can be expressed in terms of hypergeometric functions [39]. After combining the real and imaginary parts of the potential, the 3d Schrödinger equation is solved numerically to obtain the real and imaginary parts of the binding energy as a function of ξ and p_{hard} [12, 77]. The imaginary part of the binding energy is related to the width of the state

$$\Gamma(\tau, \mathbf{x}_\perp, \varsigma) = \begin{cases} 2\Im[E_{\text{bind}}(\tau, \mathbf{x}_\perp, \varsigma)] & \Re[E_{\text{bind}}(\tau, \mathbf{x}_\perp, \varsigma)] > 0, \\ 10 \text{ GeV} & \Re[E_{\text{bind}}(\tau, \mathbf{x}_\perp, \varsigma)] \leq 0, \end{cases} \quad (10)$$

where $\varsigma = \text{arctanh}(z/t)$ is the spatial rapidity. The value of 10 GeV in the second case is chosen to be large in order to quickly suppress states which are fully unbound (which is the case when the real part of the binding energy is negative).

2.2. Dynamical Model

The dynamical model used gives the spatio-temporal evolution of the typical transverse momentum of the plasma partons, $p_{\text{hard}}(\tau, \mathbf{x})$, and the plasma momentum-space anisotropy, $\xi(\tau, \mathbf{x})$, both of which are specified in the local rest frame of the plasma. The widths obtained from solution of the 3d Schrödinger equation are then integrated and exponentiated to compute the relative number of states remaining at a given proper time. This quantity is then averaged

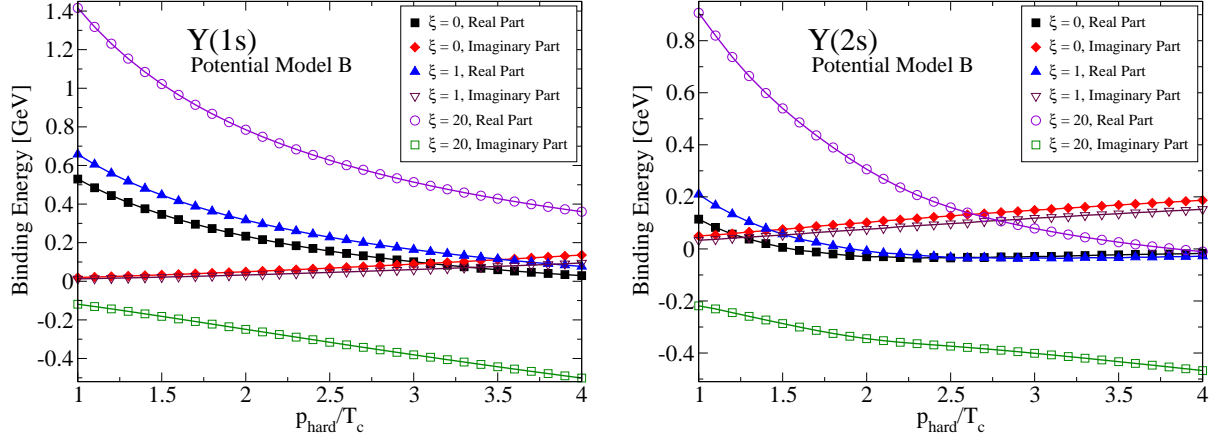


Figure 1. Real and imaginary parts of the $\Upsilon(1s)$ (left) and $\Upsilon(2s)$ (right) binding energies as a function of the hard momentum scale, p_{hard} for different levels of momentum-space anisotropy ξ .

over the transverse plane taking into account the local conditions in the plasma and weighting by the spatial probability distribution for bottomonium production which is given by the number of binary collisions computed in the Glauber model with a Woods-Saxon distribution for each nucleus. For the temporal integration the initial time is set by the formation time of the state in question. The resulting R_{AA} is a function of the transverse momentum, p_T , the rapidity ς , and the nuclear impact parameter b . To compare to experimental results transverse momentum cuts are applied assuming a $n(p_T) = n_0 E_T^{-4}$ spectrum. In addition, any cuts on the rapidity due to detector acceptance and centrality are applied as needed. For details of the dynamical model and R_{AA} computation we refer the reader to Ref. [24].

2.3. Initial conditions

For the initial conditions we use a Woods-Saxon distribution for each nucleus and determine the transverse dependence of the initial temperature via the third root of the number of participants (wounded nucleons). In the spatial rapidity direction we have investigated two possible temperature profiles: (a) a broad plateau containing a boost-invariant central region with Gaussian limited-fragmentation at large rapidity [78]

$$n(\varsigma) = n_0 \exp(-(|\varsigma| - \varsigma_{\text{flat}}/2)^2/2\sigma_\varsigma^2) \Theta(|\varsigma| - \varsigma_{\text{flat}}/2), \quad (11)$$

where $\varsigma_{\text{flat}} = 10$ is the width of the central rapidity plateau, $\sigma_\varsigma = 0.5$ is the width of the limited fragmentation tails, and n_0 is the number density at central rapidity [57]; and (b) a Gaussian motivated by low-energy fits to pion spectra

$$n(\varsigma) = n_0 \exp(-\varsigma^2/2\sigma_\varsigma^2) \quad \text{with} \quad \sigma_\varsigma^2 = 0.64 \cdot 8 c_s^2 \ln(\sqrt{s_{NN}}/2m_p)/3(1 - c_s^4), \quad (12)$$

where $c_s = 1/\sqrt{3}$ is the sound velocity, $m_p = 0.938$ GeV is the proton mass, and $\sqrt{s_{NN}}$ is the nucleon-nucleon center-of-mass energy [24, 79]. The temperature distribution is given by $T \sim n^{1/3}$. We note that Eq. (11) has the advantage that it has been tuned to successfully describe the rapidity dependence of the elliptic flow in LHC heavy ion collisions.

3. Results and Conclusions

In Fig. 1 we show the real and imaginary parts of the $\Upsilon(1s)$ and $\Upsilon(2s)$ binding energies as a function of the hard momentum scale, p_{hard} , for $\xi \in \{0, 1, 20\}$. Defining the disassociation scale

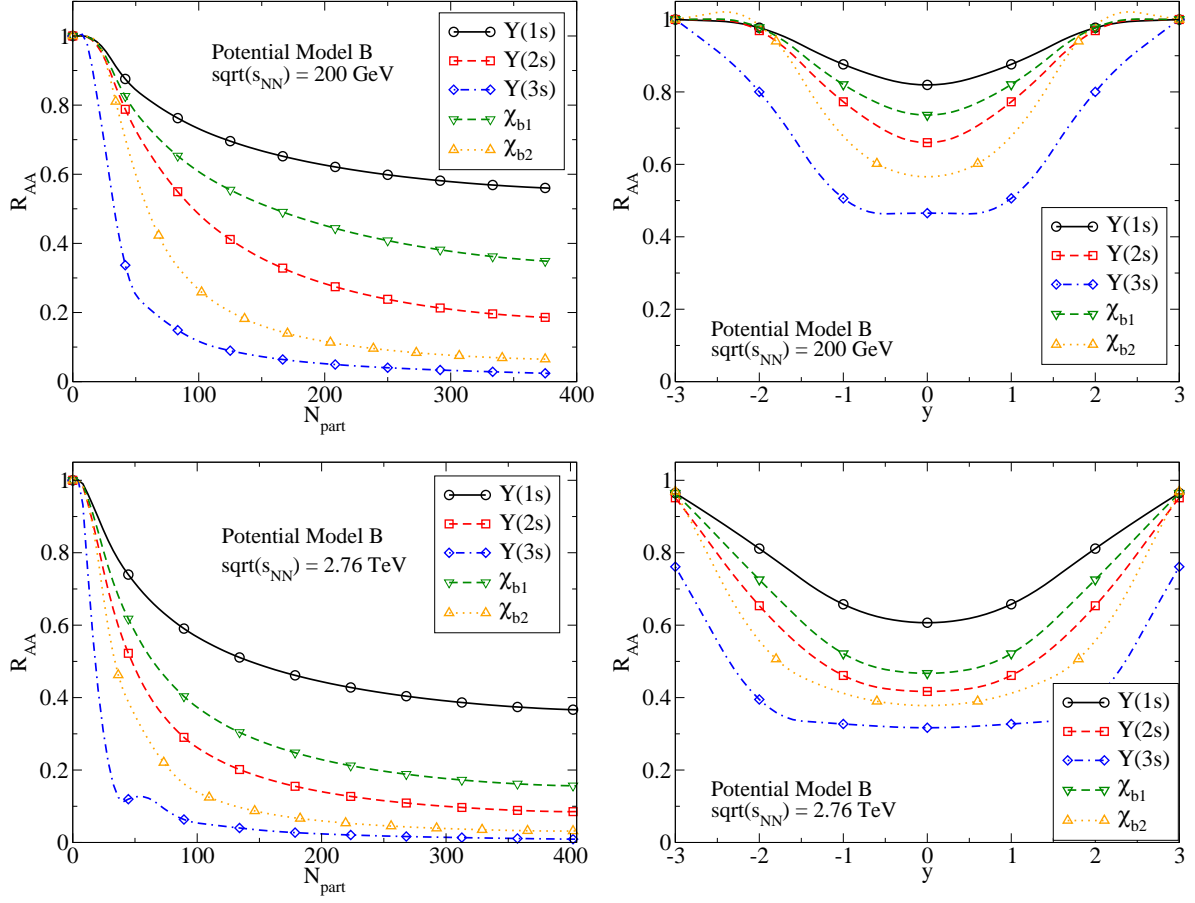


Figure 2. RHIC and LHC suppression factor R_{AA} for the $\Upsilon(1s)$, $\Upsilon(2s)$, $\Upsilon(3s)$, χ_{b1} , and χ_{b2} states as a function of the number of participants (left) and rapidity (right). In the top plots we used $\sqrt{s_{NN}} = 200$ GeV and in the bottom plots we used $\sqrt{s_{NN}} = 2.76$ TeV. In both cases, we assumed a shear viscosity to entropy density ratio of $4\pi\eta/S = 1$, and implemented cuts of $0 < p_T < 20$ GeV and (left) rapidity $|y| < 0.5$ for RHIC and $|y| < 2.4$ for LHC (right) centrality 0-100%.

as the value of p_{hard} at which the real and imaginary parts of the binding energy become equal, one finds isotropic dissociation scales of 593 MeV for the $\Upsilon(1s)$ and 228 MeV for the $\Upsilon(2s)$. In addition, as one can see from this figure, as the level of momentum space anisotropy increases, one finds that the disassociation scale increases. This means that in regions of the plasma where there is a high degree of momentum-space anisotropy, the states will be less suppressed.

In Fig. 2 we show the predicted suppression factor R_{AA} for the $\Upsilon(1s)$, $\Upsilon(2s)$, $\Upsilon(3s)$, χ_{b1} , and χ_{b2} states as a function of the number of participants (left) and rapidity (right). In this figure we see clear signs of sequential suppression, with the higher excited states having stronger suppression than the ground state. However, we note that even for states that are “melted” at relatively low central temperatures, we still obtain a non-vanishing suppression factor for these states. This is due to the fact that near the edges, where the temperature is lower, one does not see suppression of the states. Upon performing the geometrical average, we see that a large fraction of the states produced can survive even when the central temperature of the plasma is above their naive dissociation temperature.

In Fig. 3 (left) we plot $R_{AA}[\Upsilon(1s + 2s + 3s)]$ and compare with experimental data from the

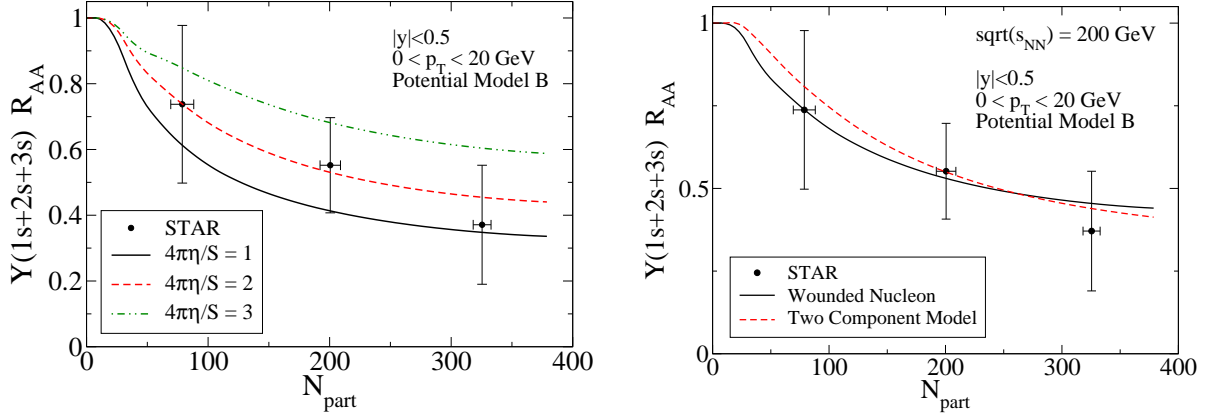


Figure 3. RHIC $\Upsilon(1s + 2s + 3s)$ suppression factor (left) compared with experimental data from the STAR Collaboration [80]. The three different lines correspond to different assumptions for the shear viscosity to entropy ratio $4\pi\eta/S \in \{1, 2, 3\}$. In both plots we used $\sqrt{s_{NN}} = 200$ GeV and implemented cuts of $0 < p_T < 20$ GeV and $|y| < 0.5$. On the right, the solid black line is the result obtained assuming wounded nucleon initial conditions and the dashed red line is the result obtained used a two component model with $\alpha = 0.145$.

STAR Collaboration [80]. As can be seen from this figure, the model does a reasonably good job of reproducing the existing STAR data for $R_{AA}[\Upsilon(1s + 2s + 3s)]$. From the left panel we can obtain an estimate of η/S : $0.08 < \eta/S < 0.24$. In Fig. 3 (right) we show the results obtained for $R_{AA}[\Upsilon(1s + 2s + 3s)]$ at RHIC energies for two different types of initial conditions (Glauber and mixed Glauber plus binary collision scaling). For both lines shown in Fig. 3 (right) we have assumed $4\pi\eta/S = 2$. Because changing the initial condition type affects particle multiplicities we have adjusted the initial temperature at RHIC energies from 433 MeV to 461 MeV in order to keep the charged particle multiplicity fixed at $dN_{ch}/dy = 620$. As can be seen from Fig. 3 (right), for peripheral collisions there is a larger dependence on the choice of initial condition type, while for central collisions the result obtained is not much affected by the choice of initial condition. This is to be contrasted with the dependence on the assumed value of η/S which affects the suppression at all centralities.

When considering the suppression of the $\Upsilon(1s)$ and $\Upsilon(2s)$ states it is important to include the effect of feed-down from higher excited states. In pp collisions only approximately 51% of $\Upsilon(1s)$ states come from direct production and similarly for the $\Upsilon(2s)$. One can compute the inclusive suppression of a state using $R_{AA}^{\text{full}}[\Upsilon(ns)] = \sum_{i \in \text{states}} f_i R_{i,AA}$ where f_i are the feed-down fractions and $R_{i,AA}$ is the direct suppression of each state which decays into the $\Upsilon(ns)$ state being considered. Here we will use $f_i = \{0.510, 0.107, 0.008, 0.27, 0.105\}$ for the $\Upsilon(1s)$, $\Upsilon(2s)$, $\Upsilon(3s)$, χ_{b1} , and χ_{b2} feed-down to $\Upsilon(1s)$, respectively [82]. For the inclusive $\Upsilon(2s)$ production we use $f_i = \{0.500, 0.500\}$ for the $\Upsilon(2s)$ and $\Upsilon(3s)$ states, respectively. For details of the computation of the direct R_{AA} for each state see Ref. [24].

In Fig. 4 we compare to recent data on the inclusive $\Upsilon(1s)$ and $\Upsilon(2s)$ suppression available from the CMS collaboration [83]. For this figure we used a broad rapidity plateau as the initial density profile as specified in Eq. (11). The central temperatures were taken to be $T_0 = \{520, 504, 494\}$ MeV at $\tau_0 = 0.3$ fm/c for $4\pi\eta/S = \{1, 2, 3\}$, respectively, in order to fix the final charged multiplicity to $dN_{ch}/dy = 1400$ in each case. As can be seen from this figure, the predictions agree reasonably well with the available data. The data seem to prefer the

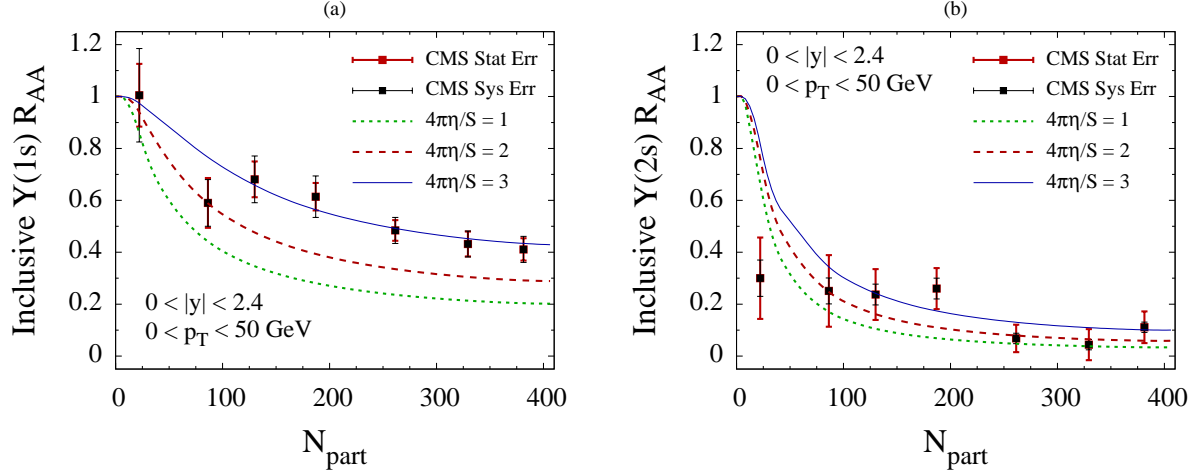


Figure 4. Predictions for the central rapidity inclusive (a) $\Upsilon(1s)$ and (b) $\Upsilon(2s)$ suppression including feed-down as a function of N_{part} along with recent data from the CMS collaboration. The three different lines correspond to different assumptions for the shear viscosity to entropy ratio $4\pi\eta/S \in \{1, 2, 3\}$.

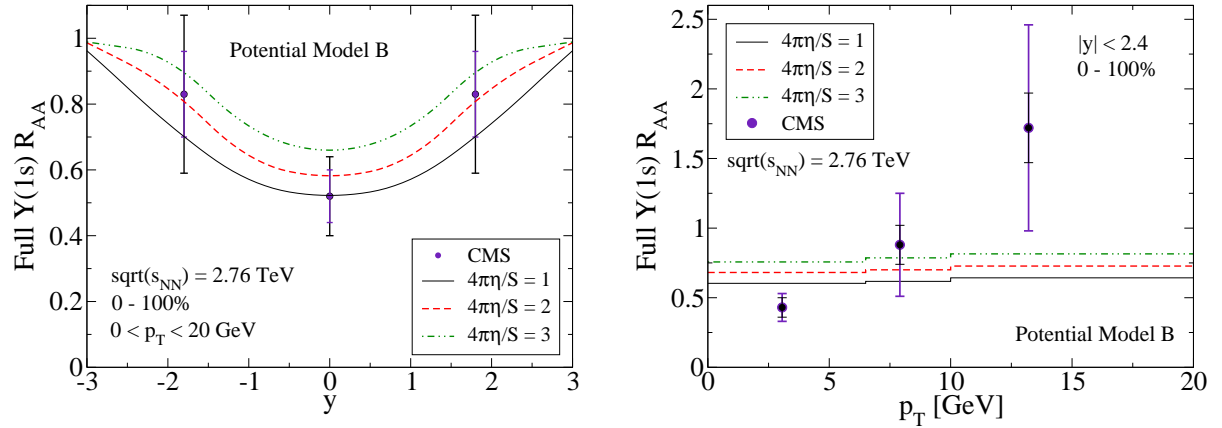


Figure 5. LHC inclusive suppression factor R_{AA} for the $\Upsilon(1s)$ including feed down effects as a function of rapidity and transverse momentum compared to experimental data from the CMS Collaboration [81].

largest value of η/S shown; however, there is a $\pm 14\%$, $\pm 21\%$ 1s, 2s global uncertainty reported by CMS, making it hard to draw firm conclusions.

In Fig. 5 we show the inclusive suppression factor $R_{AA}^{\text{full}}[\Upsilon(1s)]$. Comparing to the available CMS data [81] we can obtain an estimate for η/S at LHC energies: $0.08 < \eta/S < 0.24$ which is the same range obtained from the STAR data obtained with gold-gold collisions at lower energies. As before, more precisely determining η/S will require more data from the LHC which should be forthcoming in the near future.

4. Conclusions

In this proceedings contribution we have reviewed recent calculations of bottomonium suppression in RHIC and LHC heavy ion collisions. We presented comparisons of prior

predictions with data from the CMS Collaboration for inclusive $\Upsilon(1s)$ and $\Upsilon(2s)$ suppression and data from the STAR Collaboration for inclusive $\Upsilon(1s + 2s + 3s)$ suppression. The underlying calculations employed a complex-valued potential which incorporates both screening and in-medium dissociation of the states under consideration. We solved for the resulting real and imaginary parts of the binding energy of the $\Upsilon(1s)$, $\Upsilon(2s)$, $\Upsilon(3s)$, χ_{b1} , and χ_{b2} states. We then folded this information together with the real-time evolution of both the typical momentum of the plasma particles (p_{hard}) and their momentum-space anisotropy (ξ). We demonstrated that the resulting inclusive suppression of Υ states is in good agreement with available data. We note in closing that there are now very interesting developments concerning quarkonium in an anisotropic medium obtained employing the conjectured AdS/CFT correspondence [84–86]. These methods offer some hope to determine the temperature and momentum-space anisotropy dependence of the long range part of the potential from first principles, albeit in a theory that is not QCD.

Acknowledgments

This work was supported by NSF grant No. PHY-1068765 and the Helmholtz International Center for FAIR LOEWE program.

References

- [1] Shuryak E V 1980 *Phys. Rept.* **61** 71–158
- [2] Matsui T and Satz H 1986 *Phys. Lett.* **B178** 416
- [3] Karsch F, Mehr M T and Satz H 1988 *Z. Phys.* **C37** 617
- [4] Grandchamp L, Lumpkins S, Sun D, van Hees H and Rapp R 2006 *Phys.Rev.* **C73** 064906 (*Preprint hep-ph/0507314*)
- [5] Laine M, Philipsen O, Romatschke P and Tassler M 2007 *JHEP* **03** 054 (*Preprint hep-ph/0611300*)
- [6] Laine M 2007 *JHEP* **05** 028 (*Preprint 0704.1720*)
- [7] Dumitru A, Guo Y and Strickland M 2008 *Phys. Lett.* **B662** 37–42 (*Preprint 0711.4722*)
- [8] Rapp R, Blaschke D and Crochet P 2010 *Prog.Part.Nucl.Phys.* **65** 209–266 (*Preprint 0807.2470*)
- [9] Brambilla N, Ghiglieri J, Vairo A and Petreczky P 2008 *Phys. Rev.* **D78** 014017 (*Preprint 0804.0993*)
- [10] Dumitru A, Guo Y, Mocsy A and Strickland M 2009 *Phys.Rev.* **D79** 054019 (*Preprint 0901.1998*)
- [11] Burnier Y, Laine M and Vepsalainen M 2009 *Phys.Lett.* **B678** 86–89 (*Preprint 0903.3467*)
- [12] Margotta M, McCarty K, McGahan C, Strickland M and Yager-Elorriaga D 2011 *Phys.Rev.* **D83** 105019 (*Preprint 1101.4651*)
- [13] Umeda T, Nomura K and Matsufuru H 2005 *Eur. Phys. J.* **C39S1** 9–26 (*Preprint hep-lat/0211003*)
- [14] Asakawa M and Hatsuda T 2004 *Phys. Rev. Lett.* **92** 012001 (*Preprint hep-lat/0308034*)
- [15] Datta S, Karsch F, Petreczky P and Wetzorke I 2004 *Phys. Rev.* **D69** 094507 (*Preprint hep-lat/0312037*)
- [16] Aarts G, Allton C, Oktay M B, Peardon M and Skullerud J I 2007 *Phys. Rev.* **D76** 094513 (*Preprint 0705.2198*)
- [17] Hatsuda T 2006 *PoS LAT2006* 010
- [18] Jakovac A, Petreczky P, Petrov K and Velytsky A 2007 *Phys. Rev.* **D75** 014506 (*Preprint hep-lat/0611017*)
- [19] Aarts G, Kim S, Lombardo M, Oktay M, Ryan S *et al.* 2011 *Phys.Rev.Lett.* **106** 061602 (*Preprint 1010.3725*)
- [20] Aarts G, Allton C, Kim S, Lombardo M P, Oktay M B *et al.* 2012 (*Preprint 1210.2903*)
- [21] Ding H T 2012 (*Preprint 1210.5442*)
- [22] Rakotozafindrabe A, Ferreira E G, Fleuret F, Lansberg J P and Matagne N 2012 *PoS QNP2012* 159 (*Preprint 1207.3193*)
- [23] Strickland M 2011 *Phys.Rev.Lett.* **107** 132301 (*Preprint 1106.2571*)
- [24] Strickland M and Bazow D 2012 *Nucl.Phys.* **A879** 25–58 (*Preprint 1112.2761*)
- [25] Burnier Y, Laine M and Vepsalainen M 2008 *JHEP* **0801** 043 (*Preprint 0711.1743*)
- [26] Miao C, Mocsy A and Petreczky P 2011 *Nucl. Phys.* **A855** 125–132 (*Preprint 1012.4433*)
- [27] Brambilla N, Escobedo M A, Ghiglieri J, Soto J and Vairo A 2010 *JHEP* **09** 038 (*Preprint 1007.4156*)
- [28] Escobedo M A, Soto J and Mannarelli M 2011 *Phys.Rev.* **D84** 016008 (*Preprint 1105.1249*)
- [29] Riek F and Rapp R 2011 *New J. Phys.* **13** 045007 (*Preprint 1012.0019*)
- [30] Emerick A, Zhao X and Rapp R 2012 *Eur.Phys.J.* **A48** 72 (*Preprint 1111.6537*)
- [31] Zhao X and Rapp R 2011 *Nucl.Phys.* **A859** 114–125 (*Preprint 1102.2194*)
- [32] Akamatsu Y and Rothkopf A 2012 *Phys.Rev.* **D85** 105011 (*Preprint 1110.1203*)
- [33] Florkowski W and Ryblewski R 2011 *Phys.Rev.* **C83** 034907 (*Preprint 1007.0130*)

- [34] Martinez M and Strickland M 2010 *Nucl. Phys.* **A848** 183–197 (*Preprint* 1007.0889)
- [35] Ryblewski R and Florkowski W 2011 *J.Phys.G* **G38** 015104 (*Preprint* 1007.4662)
- [36] Martinez M and Strickland M 2011 *Nucl.Phys.* **A856** 68–87 (*Preprint* 1011.3056)
- [37] Martinez M, Ryblewski R and Strickland M 2012 *Phys.Rev.* **C85** 064913 (*Preprint* 1204.1473)
- [38] Ryblewski R and Florkowski W 2012 *Phys.Rev.* **C85** 064901 (*Preprint* 1204.2624)
- [39] Dumitru A, Guo Y and Strickland M 2009 *Phys.Rev.* **D79** 114003 (*Preprint* 0903.4703)
- [40] Huovinen P, Kolb P F, Heinz U W, Ruuskanen P V and Voloshin S A 2001 *Phys. Lett.* **B503** 58–64 (*Preprint* hep-ph/0101136)
- [41] Hirano T and Tsuda K 2002 *Phys. Rev.* **C66** 054905 (*Preprint* nucl-th/0205043)
- [42] Tannenbaum M J 2006 *Rept. Prog. Phys.* **69** 2005–2060 (*Preprint* nucl-ex/0603003)
- [43] Kolb P F and Heinz U W 2003 *In* Hwa, R.C. (ed.) et al.: Quark gluon plasma 634–714 (*Preprint* nucl-th/0305084)
- [44] Muronga A 2002 *Phys. Rev. Lett.* **88** 062302 (*Preprint* nucl-th/0104064)
- [45] Muronga A 2004 *Phys. Rev.* **C69** 034903 (*Preprint* nucl-th/0309055)
- [46] Muronga A and Rischke D H 2004 (*Preprint* nucl-th/0407114)
- [47] Baier R, Romatschke P and Wiedemann U A 2006 *Phys.Rev.* **C73** 064903 (*Preprint* hep-ph/0602249)
- [48] Romatschke P and Romatschke U 2007 *Phys. Rev. Lett.* **99** 172301 (*Preprint* 0706.1522)
- [49] Baier R, Romatschke P, Son D T, Starinets A O and Stephanov M A 2008 *JHEP* **04** 100 (*Preprint* 0712.2451)
- [50] Dusling K and Teaney D 2008 *Phys. Rev.* **C77** 034905 (*Preprint* 0710.5932)
- [51] Luzum M and Romatschke P 2008 *Phys. Rev.* **C78** 034915 (*Preprint* 0804.4015)
- [52] Song H and Heinz U W 2009 *J.Phys.G* **G36** 064033 (*Preprint* 0812.4274)
- [53] El A, Xu Z and Greiner C 2010 *Phys. Rev.* **C81** 041901 (*Preprint* 0907.4500)
- [54] Denicol G, Kodama T and Koide T 2010 *J.Phys.G* **G37** 094040 (*Preprint* 1002.2394)
- [55] Denicol G, Koide T and Rischke D 2010 *Phys.Rev.Lett.* **105** 162501 (*Preprint* 1004.5013)
- [56] Schenke B, Jeon S and Gale C 2011 *Phys.Rev.Lett.* **106** 042301 (*Preprint* 1009.3244)
- [57] Schenke B, Jeon S and Gale C 2011 *Phys.Lett.* **B702** 59–63 (*Preprint* 1102.0575)
- [58] Bozek P 2011 *Phys.Lett.* **B699** 283–286 (*Preprint* 1101.1791)
- [59] Niemi H, Denicol G S, Huovinen P, Molnar E and Rischke D H 2011 *Phys.Rev.Lett.* **106** 212302 (*Preprint* 1101.2442)
- [60] Niemi H, Denicol G, Huovinen P, Molnar E and Rischke D 2012 *Phys.Rev.* **C86** 014909 (*Preprint* 1203.2452)
- [61] Bozek P and Wyskiel-Piekarska I 2012 *Phys.Rev.* **C85** 064915 (*Preprint* 1203.6513)
- [62] Denicol G, Niemi H, Molnar E and Rischke D 2012 *Phys.Rev.* **D85** 114047 (*Preprint* 1202.4551)
- [63] Martinez M and Strickland M 2009 *Phys. Rev.* **C79** 044903 (*Preprint* 0902.3834)
- [64] Chesler P M and Yaffe L G 2009 *Phys.Rev.Lett.* **102** 211601 (*Preprint* 0812.2053)
- [65] Chesler P M and Yaffe L G 2010 *Phys.Rev.* **D82** 026006 (*Preprint* 0906.4426)
- [66] Heller M P, Janik R A and Witaszczyk P 2012 *Phys.Rev.Lett.* **108** 201602 (*Preprint* 1103.3452)
- [67] Heller M P, Janik R A and Witaszczyk P 2012 *Phys.Rev.* **D85** 126002 (*Preprint* 1203.0755)
- [68] Heller M P, Mateos D, van der Schee W and Trancanelli D 2012 *Phys.Rev.Lett.* **108** 191601 (*Preprint* 1202.0981)
- [69] Wu B and Romatschke P 2011 *Int.J.Mod.Phys.* **C22** 1317–1342 (*Preprint* 1108.3715)
- [70] Chesler P M and Teaney D 2011 4 pages, one figure (*Preprint* 1112.6196)
- [71] Romatschke P and Strickland M 2003 *Phys. Rev.* **D68** 036004 (*Preprint* hep-ph/0304092)
- [72] Mrowczynski S, Rebhan A and Strickland M 2004 *Phys. Rev.* **D70** 025004 (*Preprint* hep-ph/0403256)
- [73] Romatschke P and Strickland M 2004 *Phys.Rev.* **D70** 116006 (*Preprint* hep-ph/0406188)
- [74] Schenke B and Strickland M 2006 *Phys. Rev.* **D74** 065004 (*Preprint* hep-ph/0606160)
- [75] Petreczky P 2010 *J.Phys.G* **G37** 094009 (*Preprint* 1001.5284)
- [76] Bali G S, Schilling K and Wachter A 1997 *Phys. Rev.* **D56** 2566–2589 (*Preprint* hep-lat/9703019)
- [77] Strickland M and Yager-Elorriaga D 2010 *J. Comput. Phys.* **229** 6015–6026 (*Preprint* 0904.0939)
- [78] Strickland M 2012 (*Preprint* 1207.5327)
- [79] Bleicher M 2005 (*Preprint* hep-ph/0509314)
- [80] Reed R 2011 *J.Phys.G* **G38** 124185 (*Preprint* 1109.3891)
- [81] CMS Collaboration (CMS) 2011 Quarkonium production in PbPb collisions at $\sqrt{s_{NN}}=2.76$ TeV CMS-PAS-HIN-10-006
- [82] Affolder A A *et al.* (CDF) 2000 *Phys.Rev.Lett.* **84** 2094–2099 (*Preprint* hep-ex/9910025)
- [83] Chatrchyan S *et al.* (CMS Collaboration) 2012 (*Preprint* 1208.2826)
- [84] Giataganas D 2012 *JHEP* **1207** 031 (*Preprint* 1202.4436)
- [85] Rebhan A and Steineder D 2012 *JHEP* **1208** 020 (*Preprint* 1205.4684)
- [86] Chernercoff M, Fernandez D, Mateos D and Trancanelli D 2012 (*Preprint* 1208.2672)